Contact angles of a drop pinned on an incline

Joël De Coninck
Laboratoire de Physique des Surfaces et Interfaces, Université de Mons, 20 Place du Parc, 7000 Mons, Belgium

François Dunlop and Thierry Huillet
Laboratoire de Physique Théorique et Modélisation, CNRS-UMR 8089, Université de Cergy-Pontoise, 95302 Cergy-Pontoise, France

(Received 24 October 2016; revised manuscript received 26 April 2017; published 25 May 2017)

For a drop on an incline with small tilt angle α, when the contact line is a circle of radius r, we derive the relation $mg\sin\alpha = \gamma r\frac{\pi}{2}(\cos\theta^{\min} - \cos\theta^{\max})$ at first order in α, where $\theta^{\min}$ and $\theta^{\max}$ are the contact angles at the back and at the front, m is the mass of the drop and γ the surface tension of the liquid. We revisit in this way the Furmidge model for a large range of contact angles. We also derive the same relation at first order in the Bond number $B = \rho g R^2/\gamma$, where R is the radius of the spherical cap at zero gravity. The drop profile is computed exactly in the same approximation. Results are compared with *surface evolver* simulations, showing a surprisingly large range of contact angles for applicability of first-order approximations.

DOI: 10.1103/PhysRevE.95.052805

I. INTRODUCTION

Pinning and depinning of a drop on an incline is a subject with a long history in the field of surface phenomena. See Refs. [1–4] for historical references, and see Refs. [5–19] for more recent work. Depinning and eventual roll-off of a drop on an incline have attracted renewed attention in recent years, motivated not only by fundamental understanding but also by several applications: moving droplets during condensation as controlled by the Stenocara beetle [20], wiper-free windscreen [21], transport of chemicals in a microfluidic system, etc. The roll-off angle is often used to characterize the quality of a surface: if it is small, say below 5°, the surface is considered as perfect, such as a piece of glass or silica wafer. If the roll-off angle is large, say above 10°, then the surface must be heterogeneous, physically in terms of topographical defects or chemically in terms of various species covering the surface, or for most of the industrial cases, both [22]. For superhydrophobic surfaces, this roll-off angle is of great importance. A superhydrophobic surface is indeed characterized by a receding contact angle above 135° and a roll-off angle below 10°.

The external force described here is presented as gravity but it can be generalized to many other types of force such as thermal gradient, electrical field, chemical heterogeneities. Quite often, the derived expressions or formulas are rather approximate, with a lack of symmetry leading to a limited range of validity. We are herewith willing to consider the pinning or depinning of a sessile droplet for a very large range of contact angles, including therefore the superhydrophobic case. We believe that our results will help develop more elaborate numerical simulations to study depinning on real surfaces. For the sake of clarity, let us now introduce some definitions. The advancing and receding contact angles may be viewed as follows (see Ref. [23] for background and references): consider a small piece of contact line where the three phases meet. The sum of forces parallel to the solid surface, per unit length of contact line, is perpendicular to the line and defines the local spreading coefficient $\gamma_{SV} - \gamma_{SL} - \gamma\cos\theta = \gamma(\cos\theta_Y - \cos\theta)$, where θ is the local contact angle and θ_Y is the Young angle implied by the equation. The local contact angle θ is a macroscopic quantity, with smooth variation on the macroscopic scale, because the fluid surface is smooth. The Young angle θ_Y, before averaging, follows the heterogeneity of the solid surface energies $\gamma_{\rm SV} - \gamma_{\rm SL}$ and may vary in a range $\theta_1 \leqslant \theta_Y \leqslant \theta_2$. If the local contact angle θ falls in this range then the piece of contact line will undergo positive and negative spreading coefficients and thus will be pinned. Otherwise, it will move to one side or the other, defining advancing and receding contact angles.

This is a simplified picture, notably because it deals with metastability through equilibrium macroscopic notions only, which will be wrong at the nanoscale. One should also distinguish Wenzel states wetting nanopores from Cassie-Baxter states with air pockets, etc. The advancing and receding angles θ^A and θ^R are defined experimentally. But the basic mechanism should be valid and should imply the following scenario: a drop is gently deposited on a horizontal substrate; the macroscopic contact line is a circle. Suppose the contact angle is θ_0 with $\theta^R < \theta_0 < \theta^A$. Now tilt the substrate by a small angle α. The contact angle along the contact line becomes a function of azimuth, $\theta = \theta(\varphi)$, oscillating around θ_0 and therefore satisfying $\theta^R < \theta(\varphi) < \theta^A$ for all $\varphi \in [-\pi,\pi]$. The contact line is pinned everywhere and remains circular. Upon increasing α, depending upon θ_0, the maximum of $\theta(\varphi)$ will reach θ^A or the minimum will reach θ^R and a corresponding piece of the contact line will move by a finite amount, not yet the roll-off. The remaining piece holds the drop. Upon increasing α further, eventually the remaining piece will be unable to hold the drop, with the minimum contact angle at θ^R and the maximum at θ^A: the drop will roll off. Such a scenario with three different transitions has been experimentally observed in Ref. [11] and numerically implemented in Ref. [24]. If $\theta_0 = \theta^A$ or θ^R, of course the first stage is skipped, and the circle is deformed as soon as $\alpha > 0$. The importance of the deposition history was already stressed in Refs. [17,25–27].

Here we consider the first stage, where the contact line is pinned as a circle of radius r_0. We denote $\theta_\alpha^{\max}$ and $\theta_\alpha^{\min}$ the

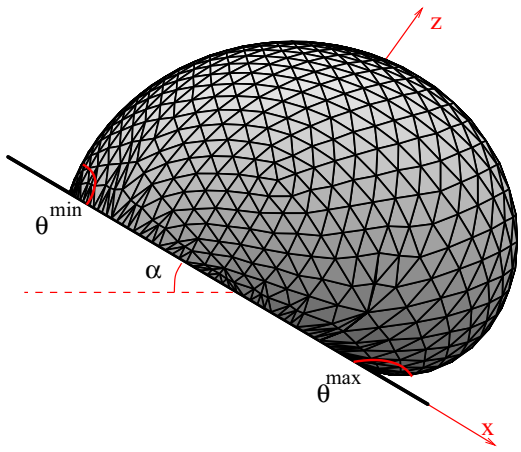

FIG. 1. Water drop on hydrophobic incline at angle $\alpha = 30^\circ$. Volume $V \simeq 42\,\mu$L. Pinned base radius $r_0 \simeq 2.0$ mm. Simulated with *surface evolver*.

contact angles at the front and at the back of the drop when the tilt angle is α (see Fig. 1). We show, for any B, for small α,

$$mg\sin\alpha = \gamma r_0 \frac{\pi}{2}\left(\cos\theta_\alpha^{\min} - \cos\theta_\alpha^{\max}\right) + O(\alpha^3), \quad (1)$$

and for any α, for small B,

$$mg\sin\alpha = \gamma r_0 \frac{\pi}{2}\left(\cos\theta_\alpha^{\min} - \cos\theta_\alpha^{\max}\right) + O(B^2), \quad (2)$$

where B is the Bond number defined in the abstract. Our derivations are analytic, but a factor $\pi/2$ or very near $\pi/2$ was found previously from numerical solutions using the finite elements method [28] or from experiments [29,30]; see Fig. 4 in Ref. [30]. We have used *surface evolver* [31] to compare first-order approximations and numerically almost exact results, showing a good agreement in the full range $0 < \theta^R < \theta_\alpha^{\min} < \theta_\alpha^{\max} < \theta^A < \pi$. For extensive applications of *surface evolver* to microdroplets; see, for instance, Refs. [32,33].

II. SESSILE DROP

We start from a sessile drop on a plane horizontal substrate, with three-phase contact-line a circle of radius r_0. We use cylindrical coordinates (z,r,φ) with origin at the center of the contact-line circle. The hydrostatic pressure just below the drop surface is $p = p_0 - \rho g z$, where p_0 is the pressure at the origin and $z = z(r)$ is the drop profile, obeying the Laplace-Young equation,

$$p - p_{\rm atm} = -2\gamma H = -\gamma\left(\frac{z''}{(1+z'^2)^{3/2}} + \frac{z'}{r\,(1+z'^2)^{1/2}}\right),$$

where γ is the liquid-air surface tension and H is the mean curvature: $2H = 1/R_1 + 1/R_2$, where R_1 and R_2 are the principal radii of curvature, with signs. The boundary conditions are $z'(0) = 0$, $z(r_0) = 0$. Eliminating the pressure gives

$$p_0 - p_{\rm atm} = \rho g z - 2\gamma H. \quad (3)$$

The parameters r_0 and $p_0 - p_{\rm atm}$ may be changed in terms of drop volume and macroscopic contact angle θ_0. This angle depends upon the way the sessile drop was deposited on the substrate and can be any angle between the receding angle and the advancing angle.

Let us now tilt the substrate by an angle α and assume that the contact line does not move, as discussed above. We keep cylindrical coordinates with z axis perpendicular to the substrate, so that the hydrostatic pressure is now

$$p = p_0 - \rho g z\cos\alpha + \rho g x\sin\alpha,$$

where the x axis is chosen in the direction of the downward slope. Then Eq. (3) becomes

$$p_0 - p_{\rm atm} = \rho g z\cos\alpha - \rho g x\sin\alpha - 2\gamma H, \quad (4)$$

where now $z = z(r,\varphi)$, with partial derivatives denoted $z_r, z_\varphi, z_{rr}, z_{r\varphi}, z_{\varphi\varphi}$, and

$$2H = \left(r^2\left(z_r^2+1\right) + z_{\varphi\varphi}^2\right)^{-3/2}\left[r z_{rr}\left(z_\varphi^2 + r^2\right) + z_r r^2\left(z_r^2+1\right) + 2z_r z_\varphi\left(z_\varphi - r z_{r\varphi}\right) + r z_{\varphi\varphi}\left(z_r^2+1\right)\right]. \quad (5)$$

At small tilt or small Bond number the solution to Eq. (4) will generally admit a Taylor expansion in a small parameter, and one may attempt to solve Eq. (4) order by order. We consider the first order, which corresponds to linearizing Eq. (4). We assume that order zero has cylindrical symmetry, so that $z(r,\varphi) = z_0(r) + \alpha z_1(r,\varphi) +$ higher orders, or a similar formula with the Bond number instead of α, and the appropriate z_0 in each case. Inserted into Eq. (5), this yields $H = H_0 + \alpha H_1 +$ higher orders or a similar formula with the Bond number instead of α, with, in any case,

$$2H_1 = \left(1+z_0'^2\right)^{-\frac{3}{2}} z_{1rr} + \left(1+z_0'^2\right)^{-\frac{1}{2}}\frac{z_{1\varphi\varphi}}{r^2} + \left(1+z_0'^2\right)^{-\frac{3}{2}}\frac{z_{1r}}{r} - 3z_0'' z_0'\left(1+z_0'^2\right)^{-\frac{5}{2}} z_{1r}. \quad (6)$$

Volume conservation and boundary conditions apply to all orders. In particular,

$$0 = \int_{-\pi}^{\pi} d\varphi \int_0^{r_0} dr\, r\, z_1(r,\varphi), \quad z_1(r_0,\varphi) = 0 \quad \forall\,\varphi.$$

III. SMALL TILT

Here we take for z_0 the solution of Eq. (3). The pressure p_0 at the center is even in α, so that $p_0 = p_{00} + O(\alpha^2)$. Order zero in Eq. (4) is Eq. (3), now written as

$$p_{00} - p_{\rm atm} = \rho g z_0 - 2\gamma H_0,$$

and the contact angle at order zero is given by $\tan\theta_0 = -z_0'(r_0)$. Order one, the coefficient of α in the Taylor expansion of Eq. (4) with $z(r,\varphi) = z_0(r) + \alpha z_1(r,\varphi) +$ higher orders, is

$$0 = \rho g z_1 - \rho g r\cos\varphi - 2\gamma H_1, \quad (7)$$

where the polar angle φ is measured from the downward slope direction. An ansatz for a solution is

$$z_1(r,\varphi) = \tilde{z}_1(r)\cos\varphi, \quad \tilde{z}_1(0) = 0, \quad \tilde{z}_1(r_0) = 0.$$

Then using Eq. (6), it appears that $\cos\varphi$ cancels out from Eq. (7), and $\tilde{z}_1(r)$ is the solution of the ordinary differential

equation,

$$\frac{\rho g r}{\gamma} = \frac{\rho g \tilde{z}_1}{\gamma} - \left(1+z_0'^2\right)^{-\frac{3}{2}} \tilde{z}_1'' - \left(1+z_0'^2\right)^{-\frac{1}{2}} \frac{\tilde{z}_1}{r^2} + \left(1+z_0'^2\right)^{-\frac{3}{2}} \frac{\tilde{z}_1'}{r} - 3 z_0'' z_0' \left(1+z_0'^2\right)^{-\frac{5}{2}} \tilde{z}_1'. \quad (8)$$

The contact angle $\theta_\alpha(\varphi)$ obeys

$$\tan\theta_\alpha(\varphi) = -\frac{\partial z}{\partial r}(r_0,\varphi) = \tan\theta_0 - \alpha \tilde{z}_1'(r_0)\cos\varphi + O(\alpha^2),$$

so that

$$\cos\theta_\alpha(\varphi) = \cos\theta_0 + \alpha \tilde{z}_1'(r_0)\sin\theta_0\cos^2\theta_0\cos\varphi + O(\alpha^2), \quad (9)$$

and

$$\frac{\cos\theta_\alpha(\varphi) - \cos\theta_\alpha^{\max}}{\cos\theta_\alpha^{\min} - \cos\theta_\alpha^{\max}} = \frac{1-\cos\varphi}{2} + O(\alpha), \quad (10)$$

to be compared to ElSherbini and Jacobi's formula [29],

$$\frac{\theta_\alpha(\varphi) - \theta_\alpha^{\min}}{\theta_\alpha^{\max} - \theta_\alpha^{\min}} = 2\frac{|\varphi|^3}{\pi^3} - 3\frac{\varphi^2}{\pi^2} + 1. \quad (11)$$

A comparison is achieved by plotting the right-hand side of Eq. (11) together with the function of φ obtained from the left-hand side of Eq. (11) with $\theta_\alpha(\varphi)$ extracted from Eq. (10) without $O(\alpha)$. The two plots are hardly distinguishable over the full range $\varphi \in [-\pi,\pi]$ when $\theta_\alpha^{\max} - \theta_\alpha^{\min}$ is small, as considered here.

The total capillary force upon the drop, projected onto the substrate and onto the direction $\varphi = \pi$, upwards along the slope, is

$$F_\gamma = -\gamma r_0 \int_{-\pi}^{\pi} d\varphi \cos\varphi \cos\theta_\alpha(\varphi) = \gamma r_0 \frac{\pi}{2}\left(\cos\theta_\alpha^{\min} - \cos\theta_\alpha^{\max}\right) + O(\alpha^3). \quad (12)$$

The error is $O(\alpha^3)$ because the part even in α cancels out when integrating over φ. Equilibrium with gravity implies $F_\gamma = mg\sin\alpha$, giving Eq. (1), implying

$$\frac{\gamma r_0 \pi\left(\cos\theta_\alpha^{\min} - \cos\theta_\alpha^{\max}\right)}{2mg\sin\alpha} = 1 + O(\alpha^2), \quad \text{as } \alpha \to 0. \quad (13)$$

Equation (9) can then be written as

$$\cos\theta_\alpha(\varphi) = \cos\theta_0 - \frac{mg\sin\alpha}{\gamma r_0 \pi}\cos\varphi + O(\alpha^2). \quad (14)$$

We have used *surface evolver* to compute the ratio Eq. (13) numerically for α varying between 0.1° and 30° for a $100\,\mu$l droplet with base radius 6 mm, corresponding to $\theta_0 \simeq 32^\circ$; see Fig. 2(a). Maximum and minimum contact angles, in the plane of symmetry of the drop, were measured by a quadratic fit with three points nearest to the contact line. The error on the ratio is inversely proportional to the number of *surface evolver* vertices times $\sin\alpha$. For α greater than 5°, error bars are too small to be shown. For α smaller than 5°, the limiting value 1 or a value derived from the quadratic fit are better. The value 0.9995 for $\alpha = 0.1^\circ$ compared to 1.00003 for $\alpha = 1^\circ$ illustrates the divergence of the error as $\alpha \searrow 0$.

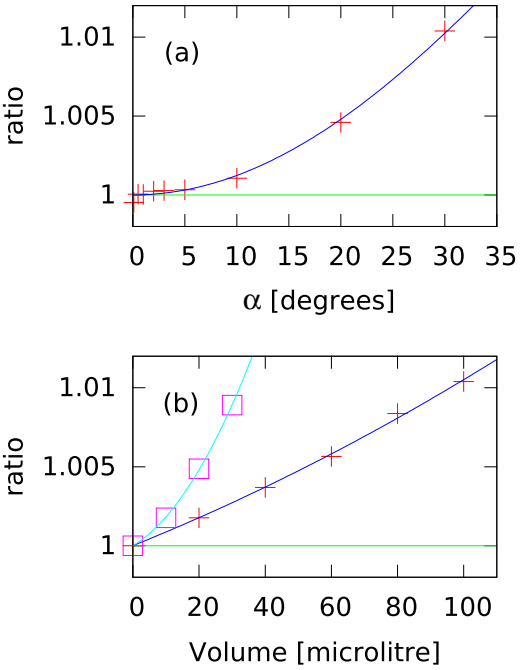

FIG. 2. The ratio Eq. (13). As (a) function of α: $100\,\mu$l droplet, with fit $1 + c\sin^2\alpha$. As (b) function of drop volume: $+(\alpha = 30^\circ)$ and $\square(\alpha = 60^\circ)$, each with fit $1 + aV + bV^2$. Simulated with *surface evolver*.

Note that to obtain Eqs. (13) and (14) it was not necessary to solve Eq. (8). Here the full profile of the drop is not computed. It will be computed for small Bond number in the next section.

IV. SMALL BOND NUMBER

The Bond number is a dimensionless ratio between gravitation and capillarity, such as $mg/(\gamma r_0)$, but more often in the form $\rho g L^2/\gamma$, where popular choices for the length L are r_0 or $V^{1/3}$ or R, related by the spherical cap formula,

$$V = \pi R^3\left(\tfrac{2}{3} - \cos\theta_0 + \tfrac{1}{3}\cos^3\theta_0\right), \quad r_0 = R\sin\theta_0,$$

where θ_0 is the contact angle. All Bond numbers generally give the same order of magnitude, but must be specified for quantitative comparisons. Here we choose $B = \rho g R^2/\gamma$ for algebraic simplicity. The drop profile at $g = 0$ is independent of the tilt,

$$z_{00} = \sqrt{R^2 - r^2} - \sqrt{R^2 - r_0^2}, \quad (15)$$

and the corresponding curvature, and the pressure at the origin, are

$$H_0 = -\frac{1}{R}, \quad p_{00} = p_{\text{atm}} + \frac{2\gamma}{R}. \quad (16)$$

We now assume a Taylor expansion $z(r,\varphi) = z_{00}(r) + Bz_1(r,\varphi) + O(B^2)$, which inserted into Eq. (5) yields

$$H = -\frac{1}{R} + BH_1 + O(B^2), \quad (17)$$

with H_1 given by Eq. (6) with z_{00} instead of z_0, which using Eq. (15) simplifies to

$$2H_1 = (1-t)^{3/2} z_{1rr} + (1-t)^{1/2} \frac{z_{1\varphi\varphi}}{r^2} + (1-t)^{1/2}(1-4t)\frac{z_{1r}}{r}, \tag{18}$$

where $t = r^2/R^2$. We then define a dimensionless first-order pressure correction p_1 by

$$p_0 - p_{\rm atm} = \frac{2\gamma}{R} + B\frac{\gamma}{R}\, p_1 \cos\alpha + \text{higher orders}. \tag{19}$$

Order one in Eq. (4) takes the form

$$p_1 \cos\alpha = \frac{z_{00}}{R}\cos\alpha - \frac{r}{R}\sin\alpha\,\cos\varphi - 2RH_1. \tag{20}$$

Equation (4) is invariant under $\alpha \to -\alpha$, $\varphi \to \pi - \varphi$, one can separate odd and even parts of $z - z_{00}$. Accordingly, at first order, we try the ansatz

$$z_1(r,\varphi) = z_{01}(r)\cos\alpha + z_{11}(r)\sin\alpha\,\cos\varphi. \tag{21}$$

Since Eq. (20) is linear and the two terms in Eq. (21) are linearly independent, it yields two independent differential equations, where $\cos\alpha$ and $\sin\alpha\,\cos\varphi$ factor out,

$$p_1 = \frac{z_{00}}{R} - 2RH_{01}, \quad 0 = 2\pi\int_0^{r_0} dr\, r z_{01},\ z_{01}(r_0) = 0, \tag{22}$$

$$0 = -\frac{r}{R} - 2RH_{11}, \quad z_{11}(0) = 0, \quad z_{11}(r_0) = 0, \tag{23}$$

where $2H_{01}$ is Eq. (18) for z_{01} instead of z_1, without the $z_{1\varphi\varphi}$ term, and

$$2\,H_{11} = (1-t)^{3/2} z_{11}'' - (1-t)^{1/2}\frac{z_{11}}{r^2} + (1-t)^{1/2}(1-4t)\frac{z_{11}'}{r}.$$

Like the small tilt case, Eqs. (21), (22), and (23) imply Eq. (2),

$$\frac{\gamma r_0 \pi\left(\cos\theta_\alpha^{\min} - \cos\theta_\alpha^{\max}\right)}{2mg\sin\alpha} = 1 + O(B) \quad \text{as } B \to 0. \tag{24}$$

We have used *surface evolver* to compute the ratio Eq. (24) numerically for $\alpha = 30^\circ$ and $\alpha = 60^\circ$ as function of volume V, when the contact angle at $g = 0$ is $\theta_0 \simeq 32^\circ$, see Fig. 2(b), where $B = B(V) = 17.2 \times (V/100)^{2/3}$. It is remarkable that the ratio Eq. (24) remains within 1% of its small B limit up to $V = 100\,\mu$l, corresponding to $B = 17.2$. This may be due in part to the smallness of $\sin\alpha = 0.5$, the correction being $O(\alpha^2)$; see Eq. (13) and the remark before it.

Equations (22) and (23) can be solved exactly. In Eq. (23) the change of variable $t = r^2/R^2$ and function $v = r z_{11}/R^2$ leads to

$$(1-t)^{-1/2} = -4(1-t)v'' + 6v' - 2\frac{v}{t},$$

$$v(0) = 0, \quad v(t_0) = 0.$$

Mathematica gives the solution

$$v = t(1-t)^{-1/2} C_1 + \tfrac{1}{3} - \tfrac{1}{3}(1-t)^{1/2} + \tfrac{1}{3}t(1-t)^{-1/2}\ln[1+(1-t)^{1/2}], \tag{25}$$

where C_1 is fixed by $v(t_0) = 0$. Equation (22) was solved in Ref. [34]. We give here an equivalent solution:

$$z_{01}'' + r^{-1}(1-t)^{-1}(1-4t)z_{01}' = R^{-2}(1-t)^{-3/2}(z_{00} - Rp_1),$$

or, with $u = z_{01}' r/R$ and $t_0 = r_0^2/R^2$,

$$2\,u' - \frac{3u}{1-t} = (1-t)^{-1} - [(1-t_0)^{1/2} + p_1](1-t)^{-3/2}.$$

This is a first-order linear differential equation, which can be solved by the variation of constants method, yielding

$$u(t) = \tfrac{1}{3}(1-t)^{-3/2} - \tfrac{1}{3} - \tfrac{1}{2}\left[(1-t_0)^{1/2} + p_1\right] t(1-t)^{-3/2}.$$

The volume of the drop does not vary:

$$0 = 2\pi\int_0^{r_0} dr\, r z_{01} = -\pi\int_0^{r_0} dr\, r^2 z_{01}' = -\frac{\pi R^3}{2}\int_0^{t_0} dt\, u,$$

implying

$$p_1 = \frac{\frac{8}{3} - 2t_0 + (1-t_0)^{1/2}\left(\frac{2t_0}{3} - \frac{8}{3}\right)}{2 - t_0 - 2(1-t_0)^{1/2}}. \tag{26}$$

Then,

$$z_{01}(r) = \int_{r_0}^{r} d\ell\, z_{01}'(\ell) = \frac{R}{2}\int_{t_0}^{t} ds\,\frac{u(s)}{s} = \frac{R}{2}\left(\frac{I}{3} + J\right), \tag{27}$$

where

$$I = 2(1-t)^{-1/2} - 2(1-t_0)^{-1/2} - 2\log\left[\frac{1+(1-t)^{1/2}}{1+(1-t_0)^{1/2}}\right],$$

$$J = [(1-t_0)^{1/2} + p_1][(1-t_0)^{-1/2} - (1-t)^{-1/2}].$$

Resulting $z = z_{00} + Bz_{01}\cos\alpha + Bz_{11}\sin\alpha\,\cos\varphi$ with z_{01} given by Eq. (27) and $z_{11} = vR^2/r$ given by Eq. (25) are shown on Fig. 3 as "first order," together with the spherical cap z_{00} and the almost exact *surface evolver* results. Comparing with Fig. 2(b), it appears that the first-order approximation to the ratio has a wider applicability than the first-order approximation to the profile, which is good for $B = 5.89$, see Fig. 3(a), but poor for $B = 17.2$, see Fig. 3(b). Indeed the value 1 for the ratio requires only the functional form Eq. (21), whatever $z_{01}(r)$ and $z_{11}(r)$, whereas the profile depends on these functions.

The profile with $B = 17.2$, corresponding to the top right points for the ratio on Figs. 2(a) and 2(b), is not far from the physical limitation $\theta_\alpha^{\min} = 0$, and the first-order approximation, in fact, gives a small negative value for $\theta_\alpha^{\min}$, while *surface evolver* still gives a positive value. At some slightly larger B, the angle $\theta_\alpha^{\min}$ will reach zero, beyond which the model ceases to represent a drop on a plane incline. And similarly if $\theta_\alpha^{\max}$ reaches π.

V. OVERHANGS

The derivation so far used cylindrical coordinates and height functions $z(r,\varphi)$, which excludes overhangs and contact angles larger than $\pi/2$. Yet singularities only occur at contact angles 0 and π, beyond which a fraction of the drop profile would go into $z < 0$ if continued analytically. The laws, Eqs. (1) and (2), therefore extend to $0 < \theta^{\min} < \theta^{\max} < \pi$. As for the drop profile, the apparent singularity at $\pi/2$ disappears in spherical polar coordinates with origin at the center of the spherical cap for $B = 0$; see Fig. 4. Then with $\theta \in [0,\theta_0]$ measured from the z axis and azimuth $\varphi \in [-\pi,\pi]$, the position vector for a

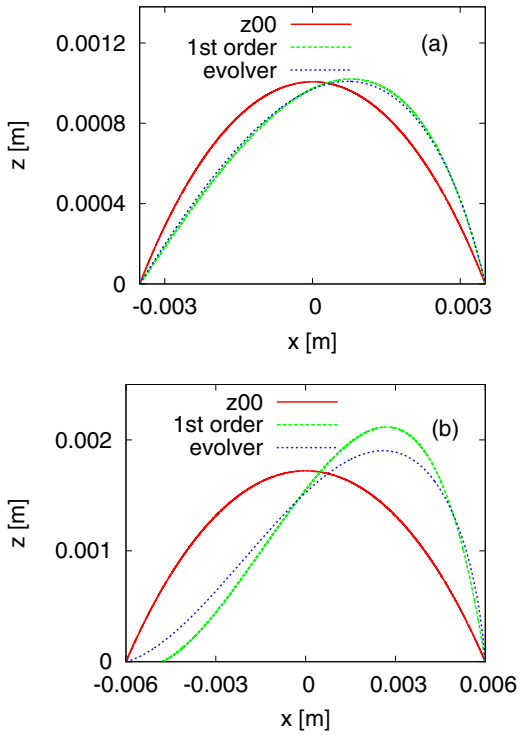

FIG. 3. Drop on 30° incline: spherical cap z_{00}, first-order $z_{00} + Bz_1$, and *surface evolver* profiles. (a) Volume 20 μl, base radius $6 \times 0.2^{1/3}$ mm, Bond number $B = 5.89$. (b) Volume 100 μl, base radius $r_0 = 6$ mm, Bond number $B = 17.2$. Abscissa x along incline, downwards, and ordinate z perpendicular to incline, both in meters.

running point on the interface is

$$\mathbf{r}\,(\theta,\varphi) = [R + \delta r(\theta,\varphi)]\mathbf{e_r}, \quad \delta r(\theta_0,\varphi) = 0,$$

where $\mathbf{e_r}$ is the radial unit vector and $r(\theta,\varphi) = R + \delta r(\theta,\varphi)$ is the new distance to the origin. New formulas are derived from the previous ones, first in the case $\theta_0 < \pi/2$ using

$$\delta r(\theta,\varphi) = Bz_{01}\cos\alpha\cos\theta + Bz_{11}\sin\alpha\cos\theta\cos\varphi,$$

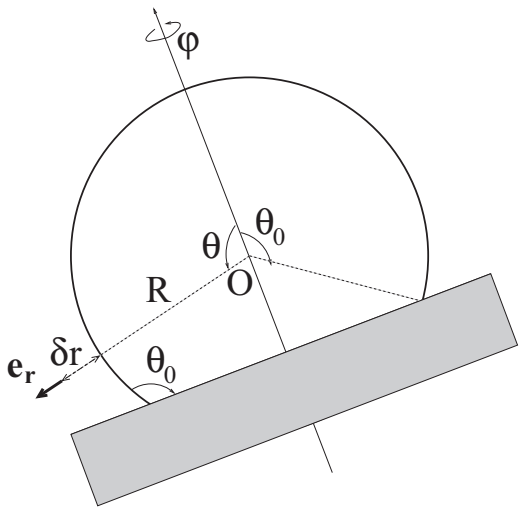

FIG. 4. Spherical coordinates.

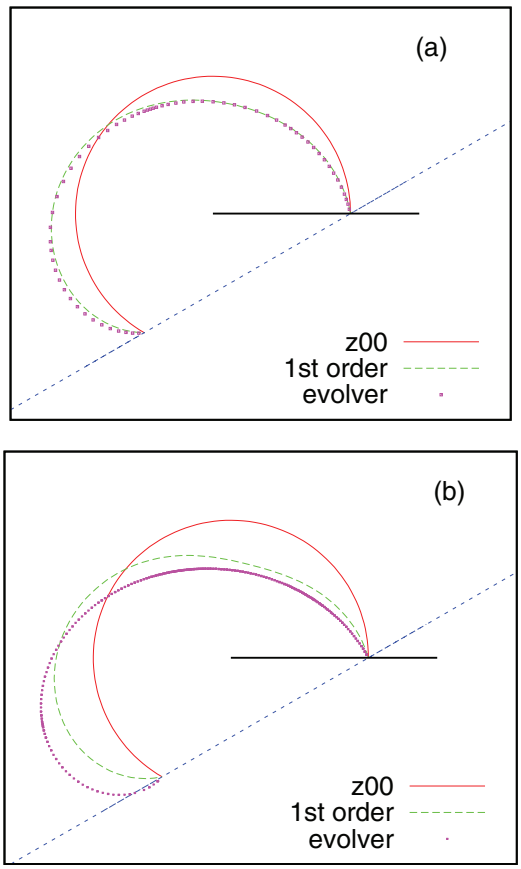

FIG. 5. Drop on 30° hydrophobic incline: spherical cap z_{00} with contact angle $2\pi/3$, first-order $z_{00} + Bz_1$ and *surface evolver* profiles. (a) Bond number $B = 0.5$, corresponding to a volume $V \simeq 25\,\mu$l and base radius $r_0 \simeq 1.7$ mm. (b) $B = 0.8$, corresponding to $V \simeq 51\,\mu$l and $r_0 \simeq 2.1$ mm. The profiles are scaled by a factor r_0^{-1} for comparison. The dimensionless radius of the contact circle is thus set to one in both figures.

and $(1 - t_0)^{1/2} = \cos\theta_0$, $(1 - t)^{1/2} = \cos\theta$. These formulas are then extended analytically to the whole range of θ with $\theta_0 \in]0,\pi[$, where the cosines can be negative. Results are shown on Fig. 5. One may note that the first order in B overestimates the effect of gravity in the hydrophilic case but underestimates it in the hydrophobic case.

VI. CONCLUSION

We have studied a drop pinned on an incline of tilt angle α, with a circular contact line and contact angle $\theta_\alpha(\varphi)$ at azimuth φ obeying

$$0 \leqslant \theta^R \leqslant \theta_\alpha^{\min} \leqslant \theta_\alpha(\varphi) \leqslant \theta_\alpha^{\max} \leqslant \theta^A \leqslant \pi, \qquad (28)$$

thus for a very large range of contact angles. Starting from the Laplace-Young equation, we have found that the first-order approximation in the tilt angle α or the Bond number B is typically within 1% of the almost exact *surface evolver* result in the full range Eq. (28), whatever the advancing and receding contact angles θ^A and θ^R. Of course, if the calculated values

of either $\theta_\alpha^{\max}$ or $\theta_\alpha^{\min}$ fall outside the interval (θ^R,θ^A), then the corresponding region of the contact line will move (recede if $\theta_\alpha^{\min} < \theta^R$ or advance if $\theta_\alpha^{\max} > \theta^A$). The exact solution of the linearized Laplace-Young equation given in the present work together with the simple Eqs. (1) and (2) for the retentive force factor should therefore be valuable.

ACKNOWLEDGMENTS

This research was partially funded by the Inter-University Attraction Poles Programme (IAP 7/38 MicroMAST) of the Belgian Science Policy Office. The authors also thank F.R.S.-FNRS and Région Wallonne for partial support.

[1] G. Macdougall and C. Ockrent, Proc. R. Soc. London Ser. A **180**, 151 (1942).
[2] Y. I. Frenkel, Zh. Eksp. Teor. Fiz. **18**, 659 (1948); translated by V. Berejnov, http://xxx.lanl.gov/abs/physics/0503051.
[3] C. G. L. Furmidge, J. Colloid Science **17**, 309 (1962).
[4] E. B. Dussan V. and R. T.-P. Chow, J. Fluid Mech. **137**, 1 (1983).
[5] D. Richard and D. Quéré, Europhys. Lett. **48**, 286 (1999).
[6] P. Roura and J. Fort, Phys. Rev. E **64**, 011601 (2001).
[7] H.-Y. Kim, H. J. Lee, and B. H. Kang, J. Colloid Interface Sci. **247**, 372 (2002).
[8] B. Krasovitski and A. Marmur, Langmuir **21**, 3881 (2005).
[9] N. Le Grand, A. Daerr, and L. Limat, J. Fluid Mech. **541**, 293 (2005).
[10] U. Thiele and E. Knobloch, New J. Phys. **8**, 313 (2006).
[11] V. Berejnov and R. E. Thorne, Phys. Rev. E **75**, 066308 (2007).
[12] E. Pierce, F. Carmona, and A. Amirfazli, Colloids Surf. A **323**, 73 (2008).
[13] Z. Huang, X. Liao, Y. Kang, G. Yin, and Y. Yao, J. Colloid Interface Sci. **330**, 399 (2009).
[14] S. P. Thampi and R. Govindarajan, Phys. Rev. E **84**, 046304 (2011).
[15] P. Olin, S. B. Lindström, T. Pettersson, and L. Wågberg, Langmuir **29**, 9079 (2013).
[16] J. H. Snoeijer and B. Andreotti, Annu. Rev. Fluid Mech. **45**, 269 (2013).
[17] M. Musterd, V. van Steijn, C. R. Kleijn, and M. T. Kreutzer, Phys. Rev. Lett. **113**, 066104 (2014).
[18] N. Janardan and M. V. Panchagnula, Colloids Surf. A **456**, 238 (2014).
[19] D. 't Mannetje, S. Ghosh, R. Lagraauw, S. Otten, A. Pit, C. Berendsen, J. Zeegers, D. van den Ende, and F. Mugele, Nat. Commun. **5**, 3559 (2014).
[20] S.-J. Hong, C.-C. Chang, T.-H. Chou, Y.-J. Sheng, and H.-K. Tsao, J. Phys. Chem. C **116**, 26487 (2012).
[21] D. 't Mannetje, C. U. Murade, D. van den Ende, and F. Mugele, Appl. Phys. Lett. **98**, 014102 (2011).
[22] C. W. Extrand and Y. Kumagai, J. Colloid Interface Sci. **170(2)**, 515 (1995).
[23] P.-G. de Gennes, F. Brochard-Wyart, and D. Quéré, *Capillarity and Wetting Phenomena: Drops, Bubbles, Pearls, Waves* (Springer-Verlag, Berlin, 2003).
[24] C. Semprebon and M. Brinkmann, Soft Matter **10**, 3325 (2014).
[25] P. Collet, J. De Coninck, F. Dunlop, and A. Regnard, Phys. Rev. Lett. **79**, 3704 (1997).
[26] T.-H. Chou, S.-J. Hong, Y.-J. Sheng, and H.-K. Tsao, Langmuir **28**, 5158 (2012).
[27] J. A. White, M. J. Santos, M. A. Rodríguez-Valverde, and S. Velasco, Langmuir **31**, 5326 (2015).
[28] R. A. Brown, F. M. Orr, Jr., and L. E. Scriven, J. Colloid Interface Sci. **73**, 76 (1980).
[29] A. ElSherbini and A. Jacobi, J. Colloid Interface Sci. **273**, 556 (2004).
[30] A. ElSherbini and A. Jacobi, J. Colloid Interface Sci. **299**, 841 (2006).
[31] K. Brakke, *Surface Evolver Manual* (Susquehanna University, Selinsgrove, PA, 2013).
[32] J. Berthier and K. Brakke, *The Physics of Microdroplets* (Scrivener-Wiley, New York, 2012).
[33] J. Berthier, *Microdrops and Digital Microfluidics*, 2nd ed. (Elsevier, New York, 2013).
[34] A. Fatollahi, Phys. Scr. **85**, 045401 (2012).